Research Article | Vol. 25, No. 23 | 13 Nov 2017 | OPTICS EXPRESS 29135

Optics EXPRESS

Micro and nano dual-scale structures fabricated by amplitude modulation in multi-beam laser interference lithography

ZIANG ZHANG,[1,2] LITONG DONG,[1] YUNFENG DING,[1] LI LI,[1] ZHANKUN WENG,[1] AND ZUOBIN WANG[1,*]

[1]*CNM and CMN, Changchun University of Science and Technology, Changchun 130022, China*
[2]*Changchun Observatory, National Astronomical Observatory, CAS, Changchun 130117, China*
** wangz@cust.edu.cn*

Abstract: In this work, an effective method was presented to obtain a specific micro and nano dual-structures by amplitude modulation in multi-beam laser interference lithography (LIL). Moiré effect was applied to generate the amplitude modulation. The specific intensity modulation patterns can be obtained by the control of the parameter settings of incident laser beams. Both the incident angle and azimuth angle asymmetric configurations can cause the amplitude modulation in the interference optic field and the modulation period is determined by the angle offset. A four-beam LIL system was set up to fabricate patterns on photoresist and verify the method. The experimental results are in good agreement with the theoretical analysis.

© 2017 Optical Society of America under the terms of the OSA Open Access Publishing Agreement

OCIS codes: (220.3740) Lithography; (220.4000) Microstructure fabrication; (220.4241) Nanostructure fabrication; (050.6875) Three-dimensional fabrication; (220.4610) Optical fabrication; (270.1670) Coherent optical effects.

References and links

1. C. Lu and R. H. Lipson, "Interference lithography: a powerful tool for fabricating periodic structures," Laser Photonics Rev. **4**, 568–580 (2010).
2. F. Yu, P. Li, H. Shen, S. Mathur, C.-M. Lehr, U. Bakowsky, and F. Mücklich, "Laser interference lithography as a new and efficient technique for micropatterning of biopolymer surface," Biomaterials **26**(15), 2307–2312 (2005).
3. D. Xia, Z. Ku, S. C. Lee, and S. R. J. Brueck, "Nanostructures and Functional Materials Fabricated by Interferometric Lithography," Adv. Mater. **23**(2), 147–179 (2011).
4. M. Vala and J. Homola, "Multiple beam interference lithography: A tool for rapid fabrication of plasmonic arrays of arbitrary shaped nanomotifs," Opt. Express **24**(14), 15656–15665 (2016).
5. Y. Oh, J. W. Lim, J. G. Kim, H. Wang, B.-H. Kang, Y. W. Park, H. Kim, Y. J. Jang, J. Kim, D. H. Kim, and B.-K. Ju, "Plasmonic Periodic Nanodot Arrays via Laser Interference Lithography for Organic Photovoltaic Cells with >10% Efficiency," ACS Nano **10**(11), 10143–10151 (2016).
6. M. Zheng, M. Yu, Y. Liu, R. Skomski, S. H. Liou, D. J. Sellmyer, V. N. Petryakov, Y. K. Verevkin, N. I. Polushkin, and N. N. Salashchenko, "Magnetic nanodot arrays produced by direct laser interference lithography," Appl. Phys. Lett. **79**, 2606–2608 (2001).
7. Z. Zhang, Z. Wang, D. Wang, and Y. Ding, "Periodic antireflection surface structure fabricated on silicon by four-beam laser interference lithography," J. Laser Appl. **26**, 4849715 (2014).
8. S.-Z. Wu, D. Wu, J. Yao, Q.-D. Chen, J.-N. Wang, L.-G. Niu, H.-H. Fang, and H.-B. Sun, "One-step preparation of regular micropearl arrays for two-direction controllable anisotropic wetting," Langmuir **26**(14), 12012–12016 (2010).
9. Y. Oh, J. W. Lim, J. G. Kim, H. Wang, B.-H. Kang, Y. W. Park, H. Kim, Y. J. Jang, J. Kim, D. H. Kim, and B. K. Ju, "Plasmonic Periodic Nanodot Arrays via Laser Interference Lithography for Organic Photovoltaic Cells with >10% Efficiency," ACS Nano **10**(11), 10143–10151 (2016).
10. R. Murillo, H. A. van Wolferen, L. Abelmann, and J. C. Lodder, "Fabrication of patterned magnetic nanodots by laser interference lithography," Microelectron. Eng. **78–79**, 260–265 (2005).
11. A. Arriola, A. Rodriguez, N. Perez, T. Tavera, M. J. Withford, A. Fuerbach, and S. M. Olaizola, "Fabrication of high quality sub-micron Au gratings over large areas with pulsed laser interference lithography for SPR sensors," Opt. Mater. Express **2**, 1571–1579 (2012).
12. L. L. Yuan and P. R. Herman, "Laser Scanning Holographic Lithography for Flexible 3D Fabrication of Multi-Scale Integrated Nano-structures and Optical Biosensors," Sci. Rep. **6**, 22294 (2016).

#306982 https://doi.org/10.1364/OE.25.029135
Journal © 2017 Received 13 Sep 2017; revised 24 Oct 2017; accepted 24 Oct 2017; published 8 Nov 2017

13. C. S. Lim, M. H. Hong, Y. Lin, Q. Xie, B. S. Luk'yanchuk, A. S. Kumar, and M. Rahman, "Microlens array fabrication by laser interference lithography for super-resolution surface nanopatterning," Appl. Phys. Lett. **89**, 2374809 (2006).
14. X. Zhu, Y. Xu, and S. Yang, "Fabrication of 3D high index photonic crystals by holographic lithography and their fidelity," in *Photonic and Phononic Crystal Materials and Devices Ix*, A. Adibi, S. Y. Lin, and A. Scherer, eds. (2009).
15. S. Orlic, F. Bernstein, C. Kratz, and A. Schloesser, "Optical transfer function of three-dimensional photonic crystals by volume holographic recording," Appl. Phys. Lett. **103**, 4816473 (2013).
16. D. Wang, Z. Wang, Z. Zhang, Y. Yue, D. Li, and C. Maple, "Effects of polarization on four-beam laser interference lithography," Appl. Phys. Lett. **102**, 4793752 (2013).
17. M. Liu, S. Wang, and L. Jiang, "Nature-inspired superwettability systems," Nat. Rev. Mater. **2**, 201736 (2017).
18. H. Xu, N. Lu, G. Shi, D. Qi, B. Yang, H. Li, W. Xu, and L. Chi, "Biomimetic antireflective hierarchical arrays," Langmuir **27**(8), 4963–4967 (2011).
19. J. Joannopoulos, S. Johnson, J. Winn, and R. Meade, "Photonic Crystals: Molding the Flow of Light 2nd edn," Princeton University (2008).

1. Introduction

In the fabrication of micro and nano structures, LIL has become one of the most important technologies with significant advantages [1]. LIL can realize the fabrication of micro and nano periodic structures with high precision [2–4]. It is a parallel processing method and is more effective compared to other technologies such as FIBL (focused ion beam lithography), EBL (e-beam lithography) and SPL (scanning probe lithography). The common sequential technologies are hard to find the balance between the small processing scale and the processing speed. The LIL fabrication area depends on the laser beam size and intensity, and both the period and the feature size can keep precisely in a large area. In recent years, LIL has been reported for many applications with the direct or indirect method, such as photovoltaic cells, antireflection surfaces, hydrophobic surfaces, light-emitting devices, biosensors and magnetic dots [5–13]. Multi-beam LIL with the beam number over four has been reported for the direct fabrication of 2-D and 3-D photonic crystals [14, 15]. The LIL has shown great application potentials.

The local optic field of the laser beam can be redistributed by interference among the coherent laser beams in the superposed area. Parts of the field are enhanced and others are eliminated from which an interference pattern is formed. The enhancement level depends on the number of superposed coherent beams and their parameters. The pattern can be more diversity by the factor configuration of the incident coherent beams. The optical field distribution of multi-beam laser interference can be considered as a line and dot pattern plus the amplitude modulation effect generated by additional incident coherent beams when the number of beams is more than three. The more beams superposed the more complex pattern will be formed. In this work, the modulation phenomenon and its application in the fabrication of micro and nano structures were discussed. Through a systematic analysis of interference of multiple coherent beams, we learned the mechanism of the intensity modulation phenomenon. Based on the analyzed knowledge, we employed a group of experiments to make verification and obtained special intensity modulation patterns by control the parameters of the incident laser beams.

2. Optical design and simulation

For simplicity, all incident beams are considered to be plane waves with the same wavelength and intensity under the noncoplanar condition. The electric field distribution of the plane waves can be expressed as

$$\vec{E} = A\exp\left[i\left(\vec{K}\cdot\vec{r}+\varphi_0\right)\right]\vec{e} \tag{1}$$

Optics EXPRESS

where A is the real amplitude, $\vec{e}$ is the unit vector of the polarization direction, $\vec{K} = 2\pi / \lambda$ is the wave vector, $\vec{r}$ is the position vector in the propagation direction, φ_0 is the initial phase, and λ is the laser wavelength.

The intensity distribution of the multi-beam interference pattern is

$$I(\vec{r}) = \sum_{j=1}^{N} E_{0j}^2 + 2\sum_{i<j} E_{0i}E_{0j}e_{ij}\cos\left[\left(\vec{K}_i - \vec{K}_j\right)\cdot\vec{r} + \varphi_{0i} - \varphi_{0j}\right] \tag{2}$$

It can be found from Eq. (2) that the intensity distribution relies on the spatial position vector, polarization direction and initial phase difference [16]. The final intensity I is the superposition of multiple 1D two-beam interference patterns. All two-beam pairs can be coherent to each other and make the final interference pattern together when the polarization directions are not orthogonal. $C_N = N(N-1)/2$ is the number of interference beam pairs, and N is the number of beams.

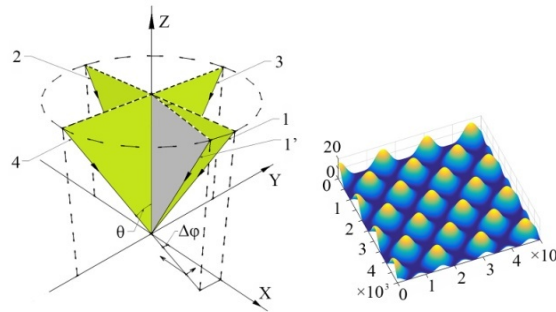

Fig. 1. Schematic diagram of four-beam LIL configuration. Beam 1' is the supposed beam vector with the azimuth angle adjustment. The right is the normal interference pattern in the Z = 0 plane.

In this work, four-beam LIL was taken as an example to analyze the amplitude modulation phenomena in multi-beam LIL. The four-beam configuration as shown in Fig. 1 is a symmetrical setup against the Z-axis. The polarization of beams 1 and 2 was the TE mode and that of beams 3 and 4 was the TM mode. The incident angles of the four beams were $\theta_1 = \theta_2 = \theta_3 = \theta_4 = \theta$. The azimuth angles were $\varphi_1 = 0^\circ$, $\varphi_2 = 180^\circ$, $\varphi_3 = 270^\circ$ and $\varphi_4 = 90^\circ$. The simulation interference pattern is shown on the right in Fig. 1. The maximum intensity can be up to $16A^2$ theoretically. The periods in the x and y directions are the same as $d_x = d_y = \lambda/2\sin\theta$.

After the incident angle of beam 1 is adjusted to θ', the beam pair in the X direction is asymmetric against the Z-axis that is the vertical axis of LIL fabrication plane. According to Eq. (1), the wave functions can be rewritten as

$$\begin{aligned} \tilde{E}_1 &= A\exp(ikx\sin\theta') \\ \tilde{E}_2 &= A\exp(-ikx\sin\theta) \\ \tilde{E}_3 &= A\exp(iky\sin\theta) \\ \tilde{E}_4 &= A\exp(-iky\sin\theta) \end{aligned} \tag{3}$$

The interference intensity distribution I can be expressed as

Optics EXPRESS

$$I = A^2 \begin{Bmatrix} 4 + 2\exp[ikx(\sin\theta + \sin\theta')] + 2\exp[ik(x\sin\theta - y\sin\theta)] \\ +2\exp[ik(x\sin\theta + y\sin\theta)] + 2\exp[ik(x\sin\theta' + y\sin\theta)] \\ +2\exp[ik(x\sin\theta' - y\sin\theta)] + 2\exp(2iky\sin\theta) \end{Bmatrix} \tag{4}$$

It can be found from Eq. (4) that there are three spatial frequencies of the pattern in the X direction, which is equivalent to the superposition of two two-beam fringe patterns with different spatial frequencies. That will generate a Moiré pattern, as shown in Fig. 2(a). The periods of the four beam interference distribution pattern in the X direction are changed to $d_x = \lambda / (\sin\theta + \sin\theta')$. There is an amplitude modulation in the X direction. The modulation frequency depends on the frequency bias of the two fringe patterns. The direction of modulation is vertical to the X-axis and the period is

$$p_x = \frac{\lambda}{|\sin\theta - \sin\theta'|} \tag{5}$$

Figure. 2(a) is the simulation result, in which the incident angle of beam 1 has an increase of $\Delta\theta_1 = 1.8^\circ$. The upper two images are 2-D intensity distributions and the lower two figures are the intensity curves at the position of Y = 0. The primary four-beam interference pattern has been modulated by beam 1 with a small change of its incident angle.

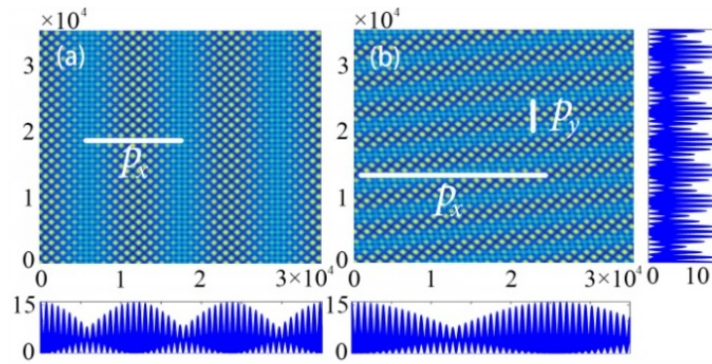

Fig. 2. Simulation result of four-beam LIL in the Z = 0 plane. (a) The incident angle is adjusted to θ' and the lower figures are the intensity profiles in the X-direction. (b) The azimuth angle is adjusted from beam 1 to beam 1' position, and the beam configuration is shown in Fig. 1. The lower and right figures are the intensity profiles in the X- and Y-directions separately.

The simulation result of the effect of incident angle offset on the modulation period as shown in Fig. 3. The incident angles changed from 2° to 60° and the angle offset changed from 0.1° to 58° with 0.1° step. The modulation period is very sensitive to the incident angle offset, which reduces rapidly with the offset increase. When the two incident angles of the asymmetric beams pair increase as shown in the figure, the same offset will lead to larger modulation periods. With a proper selection of the incident angles and angle offset, specific micro and nano dual-scale structures can be obtained. The modulation period can be widely adjusted in the range of hundreds of times of the standard interference period. If the beam pair is symmetrically configured against the Z-axis, there will be no amplitude modulation in the optical field.

Optics EXPRESS

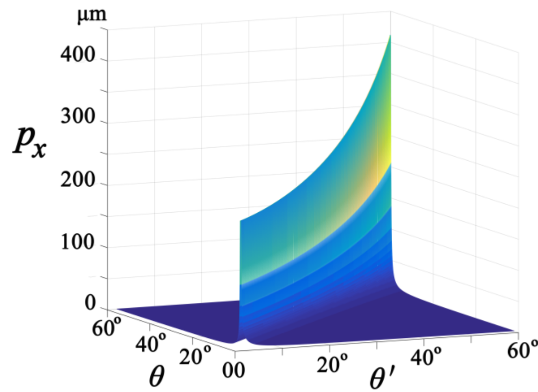

Fig. 3. The effect of incident angle offset on the modulation period. The Z-axis shows the modulation period. The X-axis and Y-axis show the incident angles of the beam pair.

It can be concluded from the above analysis that if there is a pair of asymmetric beams against to the Z-axis, the intensity modulation can be realized. Besides the incident angle, the azimuth angle can also lead to an asymmetric configuration. The azimuth angle of beam 1 is adjusted clockwise into the position of beam 1' to study the variation of the interference field, as shown in Fig. 1. In this case, the wave function of beam 1' is

$$\tilde{E}_1 = A\exp[ik(x\sin\theta\cos\varphi - y\sin\theta\sin\varphi)] \tag{6}$$

Other three beams' vectors are the same as Eq. (3). The interference I can be expressed as

$$I = A^2\begin{Bmatrix} 4+2\exp[ik(x\sin\theta\cos\varphi + y\sin\theta\sin\varphi)] + 2\exp[ik(x\sin\theta + y\sin\theta)] \\ +2\exp[ik(x\sin\theta\cos\varphi + y\sin\theta(1+\sin\varphi))] + 2\exp(2iky\sin\theta) \\ +2\exp[ik(x\sin\theta + y\sin\theta(1-\sin\varphi))] + 2\exp[ik(x\sin\theta - y\sin\theta)] \end{Bmatrix} \tag{7}$$

The simulation result is shown in Fig. 2(b). An inclined line amplitude modulation can be seen in the figure. From the simulation, the azimuth angle variation introduces two changes to the interference pattern. Firstly, the fringe direction rotates $\Delta\varphi/2$ as the same direction as beam 1. The period of the interference pattern in the X and Y directions can be calculated by

$$\begin{aligned} d_x &= \frac{\lambda}{\sin\theta(1+\cos\varphi)} \\ d_y &= \frac{\lambda}{2\sin\theta + \sin\theta\sin\varphi} \end{aligned} \tag{8}$$

Secondly, there are modulation fringes on the interference pattern in Fig. 2(b). It can be understood by vector decomposition analysis. Beam 1' can be decomposed along the X- and Y-axes. The modulation is the same as the situation caused by the incident angle variation. Both directions will generate Moiré patterns. The periods are

$$\begin{aligned} p_x &= \frac{\lambda}{\sin\theta(1-\cos\varphi)} \\ p_y &= \frac{\lambda}{\sin\theta\sin\varphi} \end{aligned} \tag{9}$$

The two direction modulations can synthesize a tilted one, and the slope of the synthesized modulation is $K = p_y / p_x$. The period of the modulation pattern is

$$p = \frac{p_x p_y}{\sqrt{p_x^2 + p_y^2}} \tag{10}$$

3. Experimental examination

For examination, an experimental LIL system was designed and built, the optical setup is shown in Fig. 4. A continuous diode pumped solid state laser (Changchun New Industries) with a single frequency and single transverse mode output was employed in the system. The laser wavelength was 360nm. A 30mm cage system (Thorlabs) was applied in the LIL system. Four coaxial thin beam splitters mounted on four hollow rotation stages and divide the laser beam into four arms. With the precise rotation around the Z axis of the four splitters separately, the azimuth angle was determined. The four incident laser beams were guided by a mechanical cage. The incident angle was co-determined by the length of the four arms and the height of the top mirrors. The incident beams filtered and expanded by spatial filters in the optical path. The initial configuration is shown in Fig. 1. The LIL system can realize the indirect micro and nano structure processing procedure through the use of photoresist as masks. The positive photoresist used in the experiment was AR-P 3740 (ALLRESIST), spin coated at 4000 rpm for 60s on the polished silicon surface. Then it was placed on a 100°C hot plate for 60s to remove the solvent. After that, it was exposed by the LIL system and developed for 60s using the developer (AR 300-26). After the cleaning and drying procedures, the surface morphology of the photoresist was characterized with the scanning electron microscope (FEI quanta 250).

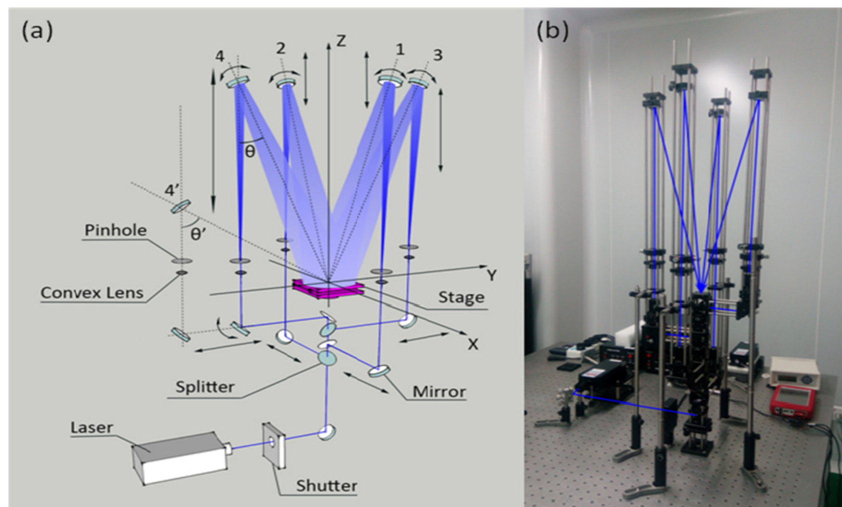

Fig. 4. The optical setup of the four-beam LIL. (a) Schematic diagram, (b) Photo of the cage system.

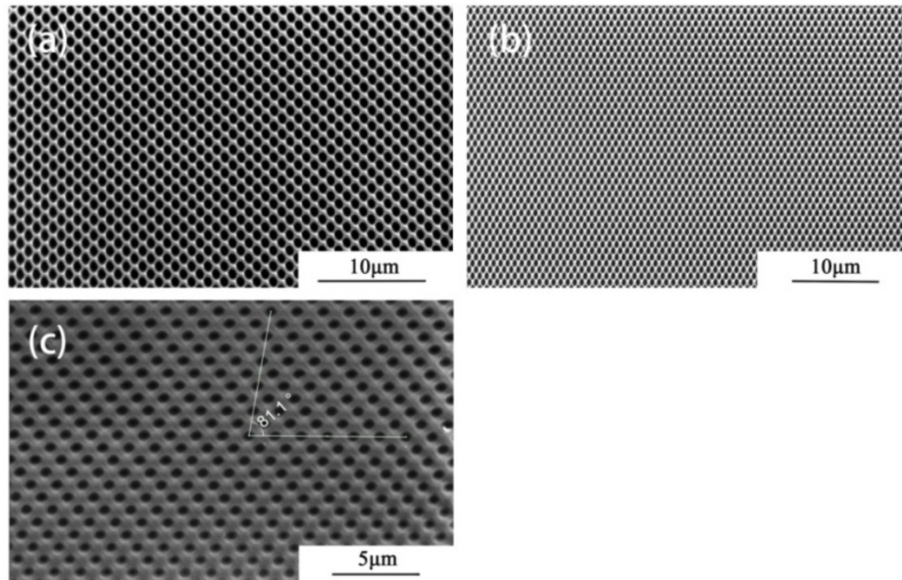

Fig. 5. Three symmetric configurations of four-beam LIL. (a) The LIL result when the four incident angles were 13.5° and the azimuth angles were $\varphi_1 = 0^\circ$, $\varphi_2 = 180^\circ$, $\varphi_3 = 270^\circ$ and $\varphi_4 = 90^\circ$. (b) The incident angles were $\theta_1 = \theta_2 = 15.5^\circ$ and $\theta_3 = \theta_4 = 13.5^\circ$, and the azimuth angles were the same as those in Fig. 1. (c) All incident angles were 13.5°, and the azimuth angles $\Delta\varphi_3 = \Delta\varphi_4 = 20^\circ$ in the clockwise direction.

In the symmetrical setup against the Z-axis configuration, there are three symmetrical cases as shown in Fig. 5. As shown in Fig. 5(a), the standard configuration without angle offset both in the two axis directions will not generate Moiré patterns. The interference pattern has maximum fringe visibility. Figure. 5(b) is the result of only changing incident angles of beam 1 and beam 2 from 13.5° to 15.5°, though the incident angles are different from the two beam pairs, that still a symmetrical setup to the Z-axis and no modulation generated. Figure. 5(c) shows another symmetrical beams configuration. The incident angles of the four beams remained the same and the azimuth angles of the beams pair of beam 3 and beam 4 were rotated 20° in the clockwise direction. It can be seen that the interference pattern also rotated but without any modulation. It can be concluded that among the three cases, in multi-beam LIL the opposite beam with a symmetrical configuration will not generate the modulation patterns although the incident and azimuth angles between the beam pairs are different. In Fig. 6(a), the incident angle of beam 1 is changed from 13.5° to 15.5°. The modulation with the period 10.7μm in the X direction can be seen clearly, and it is close to the theoretical result from Eq. (5). When the incident angles of beam 1 and beam 3 are changed to 15.5°, the synthesis modulation with the X and Y axis fringes is obtained as shown in Fig. 6(b). The azimuth angle bias influences the interference pattern that indicates in Fig. 6(c). As the azimuth change can be considered as the incident bias in the two-axis directions. As shown in Fig. 6(d), the synthesized LIL result with a clockwise rotation of 20° for beam 1 and a counterclockwise rotation of 20° for beam 4.

Optics EXPRESS

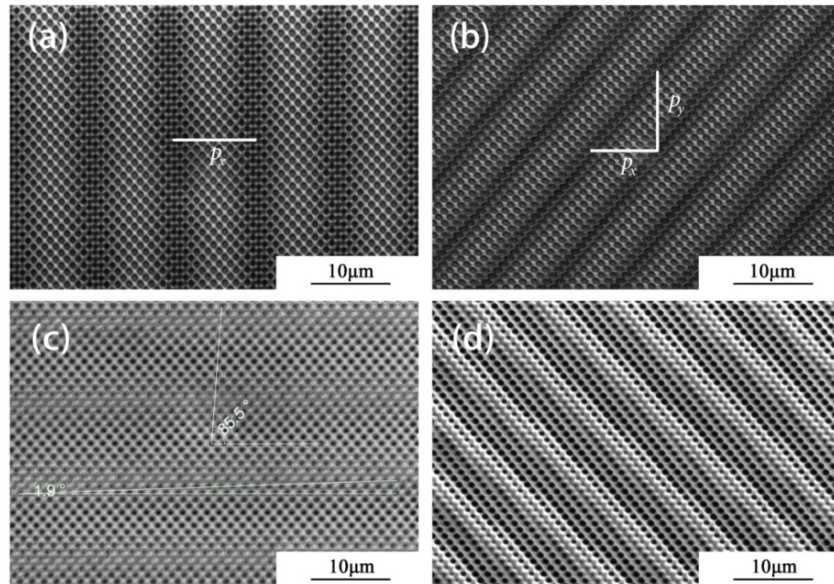

Fig. 6. Amplitude modulations generated by adjusting the incident angles and the azimuth angles separately.

4. Conclusion

In this paper, the amplitude modulation phenomena in multi-beam LIL have been studied. Through the mathematical analysis, the amplitude modulation can be consider as a kind of Moiré phenomena, and it is generated due to that the opposite beam pair is asymmetric against the Z-axis. The four-beam LIL has been taken as an example to theoretically and experimentally explore the causes. Both the incident angle and azimuth angle asymmetries can cause the amplitude modulation and the modulation period is determined by the angle offset. The experiment results have shown good correspondence with the theoretical analysis and simulation. It is an efficient way to design multiscale micro and nano interference patterns in multi-beam LIL. The amplitude modulation presents a potential to fabricate multi-scale periodic hierarchical structures with simple procedures. Through bionic research, it has been demonstrated that micro and nano two-tier structures play important roles in allowing lotus leaves to achieve both high apparent contact angles and low adhesion [17]. The moth eyes with multi-scale structures have excellent antireflection property over a wide range from UV to infrared and arouse widely interest [18]. Amplitude modulation can also find applications to create periodic line defects and wave guides in the fabrication of 2-D and 3-D photonic crystals to guide light from one location to another [19]. In the experiment, the modulation pattern is sensitive to the offsets of incident angles and azimuth angles. This raises a high requirement for the mechanical accuracy of a multi-beam LIL system to obtain fine micro and nano dual-scale structures.

Acknowledgments

This work was supported by the "111" project of China, EU FP7 (BioRA No.612641), China-EU H2020 (FabSurfWAR Nos.2016YFE0112100 and 644971), National Natural Science Foundation Program of China (Nos.61176002, 11103047, 11673082 and 11504030), and Jilin Provincial Science and Technology Program (Nos.20140414009GH, 20140622009JC, JJKHZ-2015-67, 20160520101JH, 20160101318JC and 20160623002TC).